Cholesterol Mediates Membrane Curvature during Fusion Events

Andrey Ivankin[1], **Ivan Kuzmenko**[2], **David Gidalevitz**[1],*

[1]Department of Physics and Center for Molecular Study of Condensed Soft Matter (µCoSM), Illinois Institute of Technology, Chicago, Illinois 60616

[2]Advanced Photon Source, Argonne National Laboratories, Argonne, Illinois 60439

Abstract

Biomembranes undergo extensive shape changes as they perform vital cellular functions. The mechanisms by which lipids and proteins control membrane curvature remain unclear. We use x-ray reflectivity, grazing incidence x-ray diffraction, and epifluorescence microscopy to study binding of HIV-1 glycoprotein gp41's membrane-bending domain to DPPC/cholesterol monolayers of various compositions at the air-liquid interface. The results offer a new insight into how membrane curvature could be regulated by cholesterol during fusion of the viral lipid envelope and the host cell membranes.

Cellular membranes exhibit a broad spectrum of curvatures depending on the function they perform [1,2]. Constituent and peripheral molecules can define membrane curvature in several ways: lipids of different molecular shape can distribute inhomogeneously within the bilayer [3], peripheral proteins with curved shapes can scaffold the membrane, or proteins can embed amphipathic domains shallowly into the lipid matrix [4]. At the same time, the distribution of membrane constituent molecules and activity of bending proteins depend on curvature [5-7]. The mechanism of this mechano-chemical interplay between lipids and proteins remains unclear.

Membrane penetration depth and surface area occupied by a protein's amphipathic sequence uniquely define bilayer deformations that this amphipathic region produces [8]. A sequence embedded shallowly into the polar region of a lipid bilayer expands mainly the lipid's headgroups, while the hydrocarbon chains remain undisturbed. A strong asymmetry in spacing between the tails and headgroups of the lipids leads to a positive membrane curvature [9]. When a protein's domain protrudes into the lipid membrane, it expands the lipid polar and hydrocarbon chain regions evenly and produces only negligible curvature. Recently, Campelo *et al.* proposed a quantitative description of membrane bending by rodlike inclusions [8].

The *N*-terminal fusion domain of glycoprotein gp41 is the only player of HIV-1 virus which directly interacts with the lipid bilayer of the host cell membrane and bends it via the insertion mechanism during virus entry [10]. Membrane-bending rigidity depends

*To whom correspondence should be addressed: David Gidalevitz, Department of Physics and Center for Molecular Study of Condensed Soft Matter (µCoSM), 3440 S. Dearborn Street, Chicago, IL 60616, USA. gidalevitz@iit.edu.

on cholesterol, i.e., membranes with higher cholesterol content require more energy to bend [11]. Cholesterol affects the conformation of the gp41 fusion domain favoring a β-sheet structure over α-helix [12,13]. In this Letter, we show that cholesterol also regulates membrane penetration depth and occupied surface area of the gp41 fusion domain in model Langmuir monolayer systems and thus can control curvature in biological membranes. Altogether, our present and previous [5,7] studies suggest new insights into how lipids and proteins could regulate membrane curvature.

We used epifluorescence microscopy (EFM), grazing incidence x-ray diffraction (GIXD), and x-ray reflectivity (XR) to characterize binding of the gp41 fusion domain (NH_2-AVGIGALFLGFLGAAGSTMGARS-$CONH_2$), hereafter termed FP_{23}, to model lipid membranes. The outer leaflet of the host cell membrane was mimicked with mixed dipalmitoyl-sn-glycero-3 phosphocholine (DPPC)/cholesterol Langmuir monolayers (LMs) at the air-liquid interface. The orientational order of lipid acyl chains may vary with membrane curvature and, therefore, the depth of FP_{23} insertion into planar LMs and highly curved membrane regions might not be the same. Nevertheless, we anticipate that the qualitative effect of cholesterol on the binding mode of the fusion domain should be very similar regardless of membrane curvature and studies with LMs can yield valuable insights. The surface x-ray scattering techniques employed in this study average the LM structural information across the beam footprint that leads to the requirement that the region sampled by the x-ray beam must be representative of the entire monolayer, or, in other words, the distribution of cholesterol within the model membrane should be homogeneous. We have demonstrated previously [14] that DPPC/cholesterol monolayers satisfy this requirement at the cholesterol concentrations examined. We studied monolayers with cholesterol mole fraction (χ_{CHOL}) ranging from 0 to 0.46 to account for significant inhomogeneity in the local cholesterol concentration within the cell membrane [14,15]. FP_{23} was introduced from a methanol solution into the subphase representing the extracellular fluid. The Langmuir films were prepared on Dulbecco's phosphate buffered saline subphase without calcium and magnesium (D-PBS) (Invitrogen) at 23 ± 0.2 °C at the 9-ID beam line at the Advanced Photon Source, Argonne National Laboratory (Argonne, IL). The x-ray wavelength of λ = 0.92017 Å was set by cryogenically cooled double-crystal Kozhu monochromator. More details on the methods and materials can be found in the Supplementary Material [16].

The surface area occupied by FP_{23}—

The surface area occupied by FP_{23} within the model membranes, A_{FP23}, was estimated in two steps. First, we measured the surface area change per lipid molecule, A, in DPPC/cholesterol monolayers caused by the FP_{23} insertion at the constant surface pressure of 20 mN/m, assuming that all lipid molecules in the film interact with the fusion domain. After injection of FP_{23} (0.6 μM) the mean molecular area increased by 23 $Å^2$ in the DPPC film, by 36.7 $Å^2$ in the mixed monolayer with χ_{CHOL} of 0.13, by 27.5 $Å^2$ in the film with χ_{CHOL} of 0.25, and by only 17.2 $Å^2$ in the monolayer with χ_{CHOL} of 0.46 [Fig. 1(a)].

The nonmonotonic dependence of A on the cholesterol concentration is due to the breakdown of the assumption in the cholesterol-free monolayer. Our EFM data [Fig. 1(b) and 1(c)] show that the fraction of the monolayer's surface area covered by the liquid-

disordered (LD) phase (bright regions on the EFM images) increased after FP$_{23}$ insertion from 0.5 to 0.65. This is only possible if FP$_{23}$ interacts mainly with DPPC molecules in the LD phase (roughly a half of all molecules), but not with the DPPC in the ordered domains (dark domains on the EFM images). If A is expressed in terms of area change per lipid molecule in the LD phase, its value for the cholesterol-free monolayer comprises approximately 46 Å^2 per disordered DPPC. Our diffraction data further support the idea that FP$_{23}$ does not interact with the DPPC ordered domains (see Supplementary Material [16]).

Next, we employed XR [17] to evaluate the average equilibrium lipid-to-peptide ratio, φ, in the monolayers with various χ_{CHOL}. Analysis of the reflectivity data provided the electron density (ED) profiles across the interface (Fig. 2). The XR data were analyzed using model-dependent (MD) "slab" model refinement [18,19] and model-independent (MI) stochastic fitting [20] routines, and both approaches yielded very similar results.

The ED distribution $\rho(z)$ can be used to calculate the number of electrons N^{El} in the volume occupied on average by a single lipid molecule $N^{El} = A \int_0^L \rho(z) dz$, where A is the mean molecular area [Fig. 1(a)] and L is the total thickness of the film available from the XR data analysis (Fig. 3). After FP$_{23}$ injection, the number of electrons was notably larger than that in the lipid molecules *per se* for all monolayers studied. The extra electrons N^{Extra} were therefore attributed to peptide molecules embedded into the lipid films (Table I). The lipid-to-peptide ratio, φ, can be obtained by dividing the total number of electrons in FP$_{23}$ (1738e^- assuming 50% hydration on polar groups) by N^{Extra}. We find that φ is roughly 10.6 in the DPPC monolayer, 5.8 and 6.5 in the DPPC/cholesterol films with χ_{CHOL} 0.13 and 0.25, respectively, and 10.5 in the mixture with χ_{CHOL} 0.46 (Table I). Again, since no FP$_{23}$ is present in the DPPC ordered domains (roughly a half of all molecules), the effective concentration of FP$_{23}$ in the LD phase of the cholesterol-free monolayer is twofold higher (φ is 5.3).

The area per FP$_{23}$ molecule is simply a product of φ and A (Table I). A_{FP23} comprised 245 Å^2 in DPPC, 210 Å^2 in the DPPC/cholesterol film with 13 mol% of cholesterol, and only 180 Å^2 in the other two mixed monolayers. The monomeric FP$_{23}$ can either fold into a continuous α-helix from the residue Ile4 to Met19 or form a β-sheet structure from the residue Ala1 through Gly16 [12,13]. We estimate that the structural portion of FP$_{23}$ occupies the maximum surface area of approximately 10 Å (α-helix diameter) 1.5 Å (distance between residues) $\times$16 (number of residues) = 240 Å^2 in the α-helical conformation or 3.5 Å (width of a β strand) $\times$3.3 Å (distance between residues) $\times$16 (number of residues) = 185 Å^2 in the β-strand form. The remaining FP$_{23}$ residues adopt no defined conformation and can fill the gaps between the lipids without causing substantial surface area perturbations. As anticipated, fewer FP$_{23}$ molecules insert into a monolayer (φ goes up) and they occupy smaller surface area, presumably changing the conformation, as the concentration of cholesterol increases and the hydrophobic region of the monolayer becomes more densely packed [14].

The depth of FP$_{23}$ insertion—

Further analysis of the XR data evaluates the depth of FP$_{23}$ insertion into the monolayers. The ED profiles obtained for the DPPC/cholesterol films after FP$_{23}$ injection can be divided into three regions commonly referred to as slabs. Each of these slabs is associated with a particular molecular region of DPPC and cholesterol and is characterized by its individual thickness (L_i) and average electron density (ρ_i) (Fig. 3). The ED of a slab without FP$_{23}$ can be calculated as the number of electrons from the corresponding lipid regions divided by the volume these electrons occupy $V = L_i \cdot A$, where A is the mean molecular area after FP$_{23}$ injection (Fig. 1). When the calculated ED from lipids in a slab is lower than the measured ED, we claim that FP$_{23}$ is present in this slab.

For instance, the middle slab, slab 2, of the mixture with χ_{CHOL} of 0.13 contains cholesterol ring structure ($142e^-$) and 9.3/(9.3 + 6.4) portion of the DPPC acyl chains ($242e^-$ per two chains). The molecular volume is occupied on average by 0.13 molecule of cholesterol and 0.87 molecule of DPPC. Therefore, slab 2 is expected to have $0.13 \times 142e^- + 9.3/(9.3 + 6.4) \times 0.87 \times 242e^- \approx 143.2e^-$ solely from lipids. The volume in which these electrons are confined is $V = L_2 \times A = 9.3\text{ Å} \times 84.4\text{ Å}^2 \approx 784.9\text{ Å}^3$. The corresponding ED from lipids in this slab is $\rho_2 = 143.2e^-/784.9\text{ Å}^3 \approx 0.182e^-/\text{Å}^3$ that is considerably lower than the experimental ED of $0.377e^-/\text{Å}^3$ (Fig. 3). We attribute this extra ED to FP$_{23}$.

The experimental EDs were consistently higher than that expected from lipids in all three slabs of the mixed monolayers after FP$_{23}$ injection (Fig. 3). In the DPPC monolayer, however, no extra ED from FP$_{23}$ was detected in the top ~12 Å of the phospholipid hydrocarbon chains (Fig. 3). Recently, Tristram-Nagle, *et al.* showed using oriented lipid bilayer stacks and x-ray scattering that FP23 inserts into the hydrocarbon chains region of both unsaturated dideoylphos-phatidylcholine (DOPC) and DOPC:cholesterol (7:3) model membranes [21]. Our analysis offers a further refinement of the FP23 position within the hydrophobic core of the lipid membranes without requiring an assumption about the volume of the fusion domain. We conclude that the gp41 fusion domain inserts shallowly into the monolayer without cholesterol, while it propagates across the entire thickness of the mixed films.

In these calculations, we assumed that the vertical position of cholesterol within the monolayer remains unchanged relative to DPPC after FP$_{23}$ insertion. Yet, even if cholesterol lowers to the headgroup region of DPPC upon FP$_{23}$ insertion, our conclusions stand (see Supplementary Material [16]).

A peptide needs to create a cavity within the lipid layer upon insertion into the membrane. The energy cost of changing the membrane surface area is directly proportional to the area compressibility modulus (K_A) of the bilayer [11]. While K_A value is only slightly affected by the molecular shape of the membrane phospholipids (head-group size and hydrocarbon chain unsaturation), the presence of cholesterol increases K_A significantly, thereby raising the energy cost of moving lipids apart. The magnitude of the free energy of binding, G, of a conformationally rigid peptide in a defined orientation should then be lower for membranes with a higher content of cholesterol. Indeed, G for the honeybee

toxin, melittin, which adopts an α-helical conformation upon binding to the lipid layer and which remains oriented parallel to the membrane interface in the presence of cholesterol [22], decreases from −7.6 kcal/mol for DOPC bilayers to −4.5 kcal/mol for the equimolar sphingomyelin/cholesterol bilayers [23].

Importantly, we find that the embedding depth and the occupied surface area of the gp41 membrane-bending domain, which exhibits conformational plasticity, depend strongly on the presence of cholesterol in the monolayers. Remarkably, our calculations of G for FP$_{23}$ (see Supplementary Material [16]) show that the reorientation and a possible conformational switch allow the fusion domain to insert into the DPPC/cholesterol monolayers with different χ_{CHOL} at the same efficiency; variations in G do not exceed 0.4 kcal/mol (Table I).

The Langmuir monolayer's curvature in our model system is fixed to zero due to the dominance of the surface tension at the air-liquid interface. However, this is not the case for lipid bilayers in biological membranes with liquid on both sides of the interface. Campelo *et al.* have demonstrated theoretically that the depth and mode of penetration of a protein into the outer leaflet (monolayer) of a lipid bilayer defines the overall curvature that this protein produces [8]. According to their analysis, when the gp41 protein domain embeds shallowly into the outer leaflet with a large expansion of area at the level of the head-groups, which is the case for low cholesterol concentrations, this will lead to a significant positive curvature in the lipid bilayer that is essential at the initial stage of the fusion pore formation (Fig. 3). In contrast, FP$_{23}$ protrudes into a monolayer with a higher cholesterol concentration and expands the hydrophobic and hydrophilic regions almost equally. FP$_{23}$ in this mode of penetration should have a milder effect on the overall curvature of the host cell membrane [8] and may represent the gp41 domain in the later stages of the fusion process. Since the difference in G between these two states is at the order of thermal fluctuations, the membrane can bend back-and-forth simply by regulating the local concentration of cholesterol at the point of contact with membrane-bending sequences, such as the gp41 fusion domain, and hence local curvature these domains produce.

One of the most puzzling questions in the field of cell membrane mechanics is: what are the mechanisms in the arsenal of biological membranes to regulate the activity of membrane-bending molecules? Curvature has recently emerged as one powerful tool in the membrane's toolkit. Amphipathic α-helices (AHs)—structural motifs of a wide range of proteins—deform a lipid bilayer by folding upon contact with the membrane and inserting their hydrophobic face in the lipid bilayer. This insertion process is defined by the local membrane curvature, as it is facilitated by curvature-induced defects in lipid packing, resulting in a higher binding affinity of AHs for positively curved membranes.

Our study offers evidence for the existence of the alternative mechanism for biological membranes to modulate deformations that membrane-bending molecules produce. The binding mode of a protein sequence and, thus, membrane curvature that it should produce depend strongly on the lipid composition at the point of contact.

Supplementary Material

Refer to Web version on PubMed Central for supplementary material.

Acknowledgments

References

[1]. Parthasarathy R and Groves JT, Soft Matter 3, 24 (2007).

[2]. Shibata Y, Hu J, Kozlov MM, and Rapoport TA, Annu. Rev. Cell Dev. Biol 25, 329 (2009). [PubMed: 19575675]

[3]. Janmey PA and Kinnunen PKJ, Trends Cell Biol. 16, 538 (2006). [PubMed: 16962778]

[4]. Zimmerberg J and Kozlov MM, Nat. Rev. Mol. Cell Biol 7, 9 (2005).

[5]. Bacia K, Schwille P, and Kurzchalia T, Proc. Natl. Acad. Sci. U.S.A 102, 3272 (2005). [PubMed: 15722414]

[6]. Roux A, Cuvelier D, Nassoy P, Prost J, Bassereau P, and Goud B, EMBO J. 24, 1537 (2005). [PubMed: 15791208]

[7]. Parthasarathy R, Yu C.-han, and Groves JT, Langmuir 22, 5095 (2006). [PubMed: 16700599]

[8]. Campelo F, McMahon HT, and Kozlov MM, Biophys. J 95, 2325 (2008). [PubMed: 18515373]

[9]. Graham TR and Kozlov MM, Curr. Opin. Cell Biol 22, 430 (2010). [PubMed: 20605711]

[10]. Wyatt R and Sodroski J, Science 280, 1884 (1998). [PubMed: 9632381]

[11]. McIntosh TJ and Simon SA, Annu. Rev. Biophys. Biomol. Struct 35, 177 (2006). [PubMed: 16689633]

[12]. Castano S and Desbat B, Biochim. Biophys. Acta 1715, 81 (2005). [PubMed: 16126160]

[13]. Qiang W and Weliky DP, Biochemistry 48, 289 (2009). [PubMed: 19093835]

[14]. Ivankin A, Kuzmenko I, and Gidalevitz D, Phys. Rev. Lett 104, 108101 (2010). [PubMed: 20366454]

[15]. Lingwood D and Simons K, Science 327, 46 (2009).

[16]. See Supplementary Material at 10.1103/PhysRevLett.108.238103 for details.

[17]. Als-Nielsen J, Jacquemain D, Kjaer K, Leveiller F, Lahav M, Leiserowitz L, Phys. Rep 246, 251 (1994).

[18]. Ivankin A, Livne L, Mor A, Caputo GA, DeGrado WF, Meron M, Lin B, Gidalevitz D, Angew. Chem., Int. Ed 49, 8462 (2010).

[19]. Neville F, Ivankin A, Konovalov O, and Gidalevitz D, Biochim. Biophys. Acta 1798, 851 (2010). [PubMed: 19800862]

[20]. Danauskas SM, Li D, Meron M, Lin B, and Lee KYC, J. Appl. Crystallogr 41, 1187 (2008).

[21]. Tristram-Nagle S, Chan R, Kooijman E, Uppamoochikkal P, Qiang W, Weliky DP, and Nagle JF, J. Mol. Biol 402, 139 (2010). [PubMed: 20655315]

[22]. Raghuraman H and Chattopadhyay A, Biosci. Rep 27, 189 (2006).

[23]. Allende D, Simon SA, and McIntosh TJ, Biophys. J 88, 1828 (2005). [PubMed: 15596510]
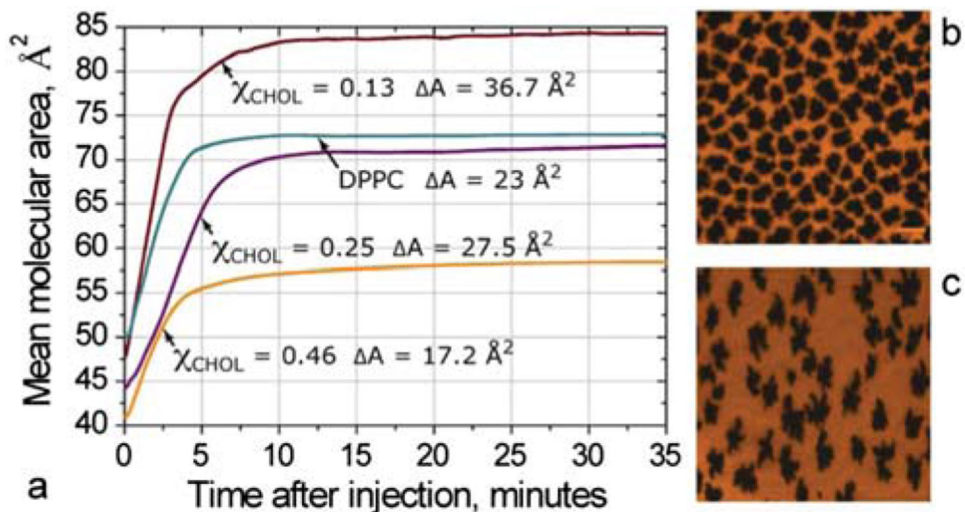
FIG. 1.
(a) Increase in the mean molecular area in the pure DPPC film and DPPC/cholesterol monolayers with χ_{CHOL} 0.13, 0.25, and 0.46 after injection of FP_{23}. (b) EFM images of DPPC before FP_{23} injection and (c) 15 minutes after. Liquid-disordered (bright) phase of DPPC covers ~50% of the area before and ~65%–70% after FP_{23} injection. This suggests that FP_{23} interacts mainly with the liquid-disordered phase of DPPC.
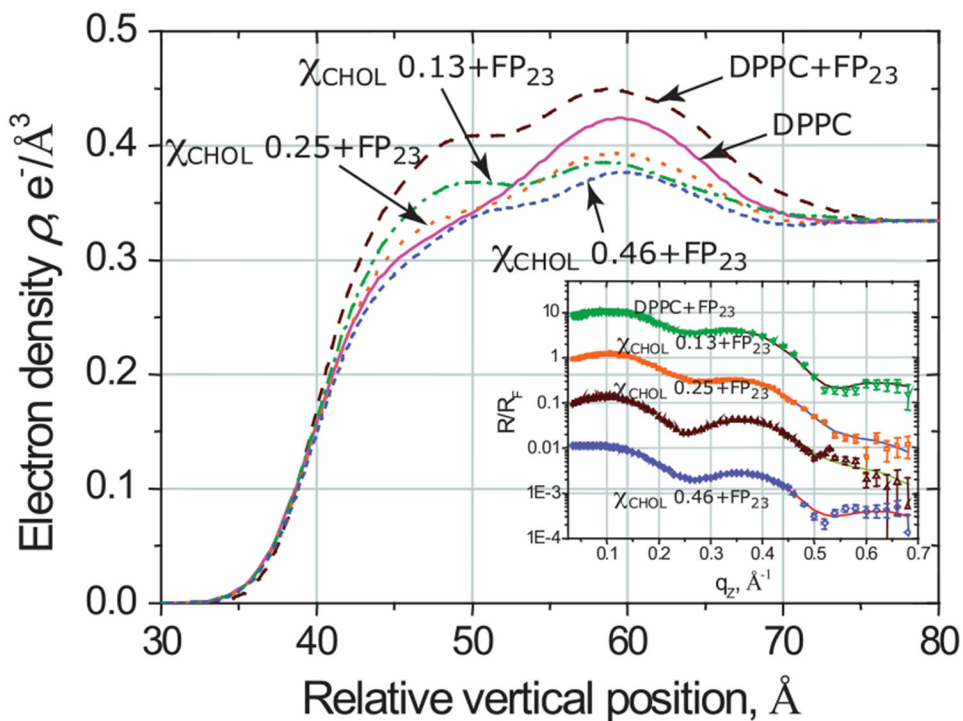
FIG. 2.

The electron density distributions in the DPPC film before injection of FP_{23} and in the DPPC and DPPC/cholesterol monolayers after FP_{23} injection perpendicular to the aqueous interface. Insert is XR data (symbols) and corresponding fits (lines) normalized by Fresnel reflectivity plotted against scattering vector q_Z. For clarity the reflectivity curves are shifter vertically.

	L_i	ED expected from lipids[a]		ED observed	Is FP$_{23}$ in there?
DPPC	11.9 Å	0.211 e⁻/Å³	>	0.192 e⁻/Å³	No
	3.9 Å	0.211 e⁻/Å³	<	0.461 e⁻/Å³	Yes
	7.9 Å	0.286 e⁻/Å³	<	0.475 e⁻/Å³	Yes
χ_{CHOL} 0.13	6.4 Å	0.175 e⁻/Å³	<	0.297 e⁻/Å³	Yes
	9.3 Å	0.182 e⁻/Å³	<	0.377 e⁻/Å³	Yes
	6.1 Å	0.279 e⁻/Å³	<	0.441 e⁻/Å³	Yes
χ_{CHOL} 0.25	6.2 Å	0.116 e⁻/Å³	<	0.308 e⁻/Å³	Yes
	10.1 Å	0.205 e⁻/Å³	<	0.355 e⁻/Å³	Yes
	7.4 Å	0.236 e⁻/Å³	<	0.437 e⁻/Å³	Yes
χ_{CHOL} 0.46	7.3 Å	0.201 e⁻/Å³	<	0.281 e⁻/Å³	Yes
	10.0 Å	0.242 e⁻/Å³	<	0.355 e⁻/Å³	Yes
	6.8 Å	0.235 e⁻/Å³	<	0.402 e⁻/Å³	Yes

gp$_{41}$ domain

DPPC   164 e⁻   242 e⁻
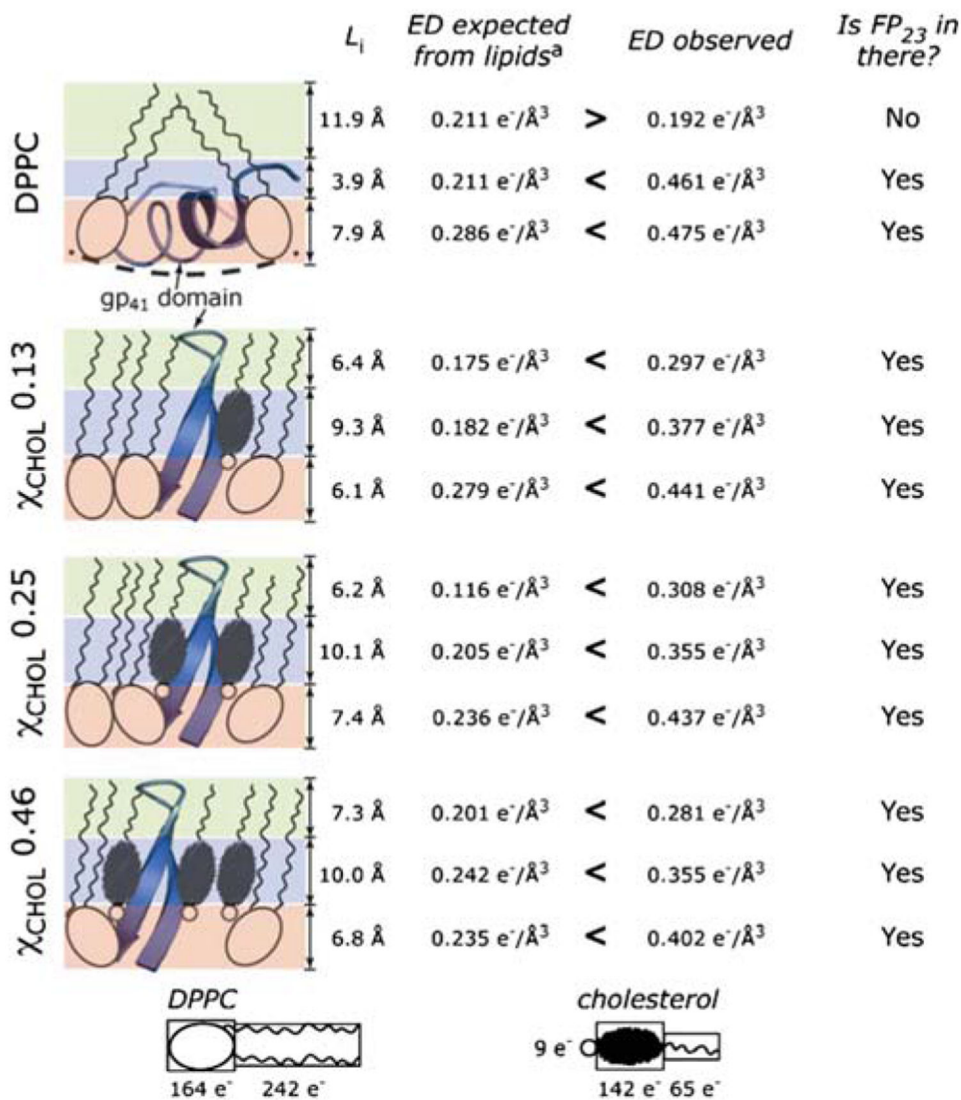
cholesterol   9 e⁻   142 e⁻ 65 e⁻

FIG. 3.
Results of the XR data analysis from left to right: cartoon schematics of the out-of-plane molecular arrangement of DPPC, cholesterol, and FP$_{23}$ and of the slab association; thicknesses of the corresponding slabs, L_i; The contribution of lipids to the ED of a slab; Experimental ED in a slab. FP$_{23}$ is depicted as an α-helix in the DPPC film and as a β-turn in DPPC/cholesterol monolayers based on the previous reports [12,13].

TABLE I.

Membrane binding properties of FP_{23}.

Sample	[a] N_{Extra}, e^-	[b] φ	[c] A_{FP23}, Å^2	[d] G, kcal mol^{-1}
DPPC + FP_{23}	163.6	[e] 5.3	245	[e] −8.05
DPPC/Chol(87:13) + FP_{23}	302.1	5.8	210	−8.02
DPPC/Chol(75:25) + FP_{23}	266.5	6.5	180	−8.00
DPPC/Chol(54:46) + FP_{23}	165.7	10.5	180	−7.79

[a] N_{Extra} is a number of FP_{23} electrons in the volume occupied by a single lipid molecule.

[b] φ denotes the equilibrium lipid-to-peptide ratio in the monolayers.

[c] A FP_{23} is the area per FP_{23} monomer within a film.

[d] G-Gibbs free energy of FP_{23} binding to the monolayers.

[e] This value accounts for the fact that only 50% of DPPC molecules interact directly with FP_{23}.